Journal of Physical Organic Chemistry

WILEY

Journal of Physical Organic Chemistry

RESEARCH ARTICLE OPEN ACCESS

Composite Single-Reference and Explicitly Correlated Multireference Calculations on the Mechanism of Pyrrole Pyrolysis

Barry K. Carpenter

School of Chemistry, Cardiff University, Cardiff, UK

Correspondence: Barry K. Carpenter (carpenterb1@cardiff.ac.uk)

Received: 20 November 2025 | **Revised:** 22 January 2026 | **Accepted:** 28 January 2026

ABSTRACT

The pyrolysis of pyrrole has previously been studied in shock-tube experiments and in jet-stirred reactors. The results have been interpreted with the aid of density functional and ab initio electronic-structure calculations, in combination with kinetic models. The present work has sought to reinvestigate the mechanism and kinetics using more sophisticated electronic structure calculations and a multiwell master equation kinetic model. The intent has been not only to probe the reaction starting with pyrrole at high temperature and pressure but also to use the same mechanistic network to examine the reaction of allyl radical with •CN at low temperature and pressure. The question being addressed is whether the high exothermicity of this radical combination reaction could drive formation of pyrrole in extraterrestrial environments, such as the interstellar medium or in planetary atmospheres. The results reveal that two new intermediates, not considered in previous mechanisms, play important roles in the overall chemistry. Furthermore, two previously proposed mechanistic steps are found not to be viable. The master-equation analysis reveals that only traces of pyrrole would be expected to form from allyl + •CN, despite there being enough excess kinetic energy to overcome all barriers to its formation. An explanation for this conclusion is offered.

1 | About the Honoree

I first met Matt Platz when he started his PhD studies in the group of Jerome A. Berson at Yale. This was 1973 and I was a postdoctoral research associate in the group. It was immediately apparent to me that Matt was smart, dedicated to his science, but also a warm and humorous individual. We quickly became friends, as did our wives. Not only did Matt and I learn new chemistry together but I, being fresh off the boat (figuratively speaking) from the UK, was naïve about American culture. These were momentous times in the USA, with the end of the Vietnam War and the beginning of the Watergate affair, and so I needed a good deal of guidance to understand what was going on. Matt provided that in his inimitably forthright and humorous manner. I found Matt to be a man of compassion and unshakeable integrity. Nothing in the intervening half century has caused me to change my mind on that assessment.

2 | Introduction

2.1 | Prior Experimental Results on Pyrrole Pyrolysis

The first investigation of pyrrole pyrolysis was conducted on the neat liquid at 1123 ± 5 K and reported in 1968. It produced HCN as the principal gaseous product, plus a large number of higher molecular weight compounds, including polycyclic aromatic hydrocarbons [1]. In 1989, a shock-tube study was reported by Lifshitz and coworkers [2]. They investigated the products formed behind the reflected shock wave in a temperature range of 1050–1450 K, with a residence time of approximately 2 ms. The principal products that they detected are shown in Scheme 1.

They reported two Arrhenius expressions for the overall disappearance of pyrrole, an "initiation" rate constant given by:

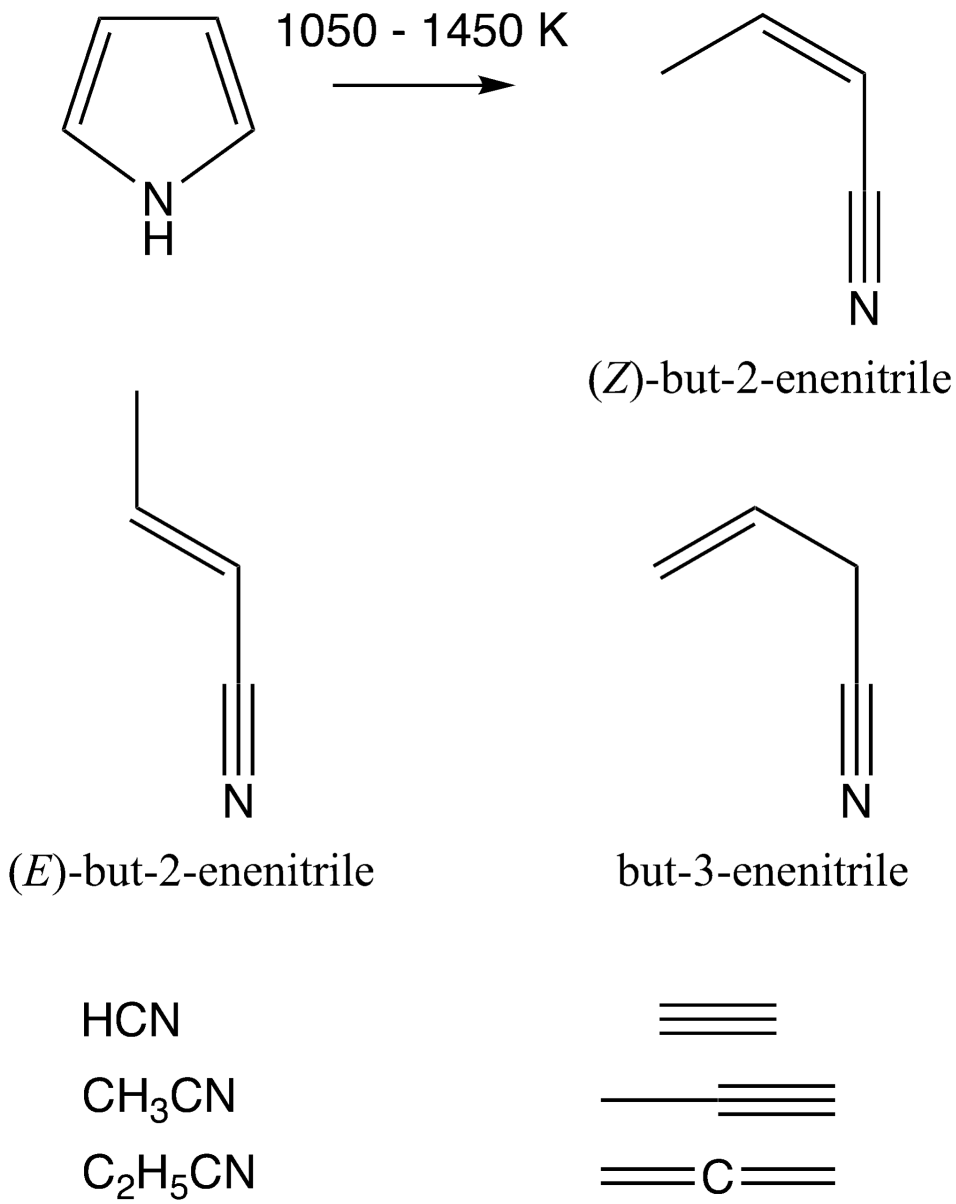

SCHEME 1 | Principal products formed in the shock-tube studies of Lifshitz et al. [2]

$$k = 10^{14.83} \times \exp\left(-75 \times 10^3 / RT\right)$$

and an "overall" rate constant, given by:

$$k = 10^{15.90} \times \exp\left(-80 \times 10^3 / RT\right).$$

For both expressions, the activation energy is in kcal/mol and the pre-exponential factor in units of s^{-1}.

They also reported apparent first-order Arrhenius expressions for formation of several of the products, as will be discussed later.

A second shock-tube study was reported in 1991 by Mackie and coworkers [3]. Their study covered the temperature range 1200–1700 K and pressures of 7.5–13.5 atm. Their residence times behind the reflected shock front ranged from 450 to 750 μs. They deduced a single Arrhenius expression (with the same units as above) for the disappearance of pyrrole, which was:

$$k = 10^{14.1\pm0.7} \times \exp\left(-74.1 \pm 3.0 \times 10^3 / RT\right).$$

They found most of the same products as Lifshitz and coworkers, but not with the same relative rates of appearance. A particular discrepancy was found for acetylene, which appeared in the same amount as propyne + allene at about 1230 K in the Lifshitz study but not until nearly 1400 K in the Mackie study. Equally striking was the appearance of C_2H_5CN in the Lifshitz products but not in the Mackie products.

As Mackie et al. noted, their rate constant for disappearance of pyrrole is about five times smaller than Lifshitz's "overall" rate constant. The Arrhenius expressions reveal that the Mackie rate constant is also about four times smaller than Lifshitz's "initiation" rate constant. These discrepancies will be addressed further in the Results and Discussions section.

The most recent reports have involved pyrolysis of pyrrole in jet-stirred reactors. Both have been conducted at atmospheric pressure, one in a temperature range of 925–1200 K [4] and the other 940–1240 K [5]. The residence times in the reactors were, respectively, 2 and 3 s, and so at least three orders of magnitude longer than in the shock-tube experiments. Perhaps surprisingly, one of the principal products detected in both studies was methane, formed in much greater quantities than propyne, allene, or any of the butenenitrile isomers. In the two shock-tube studies, methane was at best a trace product. The only credible mechanism for formation of methane from pyrrole involves a radical-chain sequence, as indeed the authors of both studies propose [4, 5]. The problem for understanding the mechanism of pyrrole pyrolysis is that radical chains can be initiated by trace impurities (notably oxygen) and are likely to play a significant role when the reactants are held at high temperature for a relatively long time. It is thus difficult to extract much useful information about nonradical pathways in the pyrrole pyrolysis mechanism from the jet-stirred reactor results.

2.2 | Prior Computational Results and Mechanistic Proposals for Pyrrole Pyrolysis

A rudimentary mechanism for the pyrolysis of pyrrole was proposed by Lifshitz et al. in their original paper on the shock tube experiments [2]. It suggested a central role for the diradical **11**

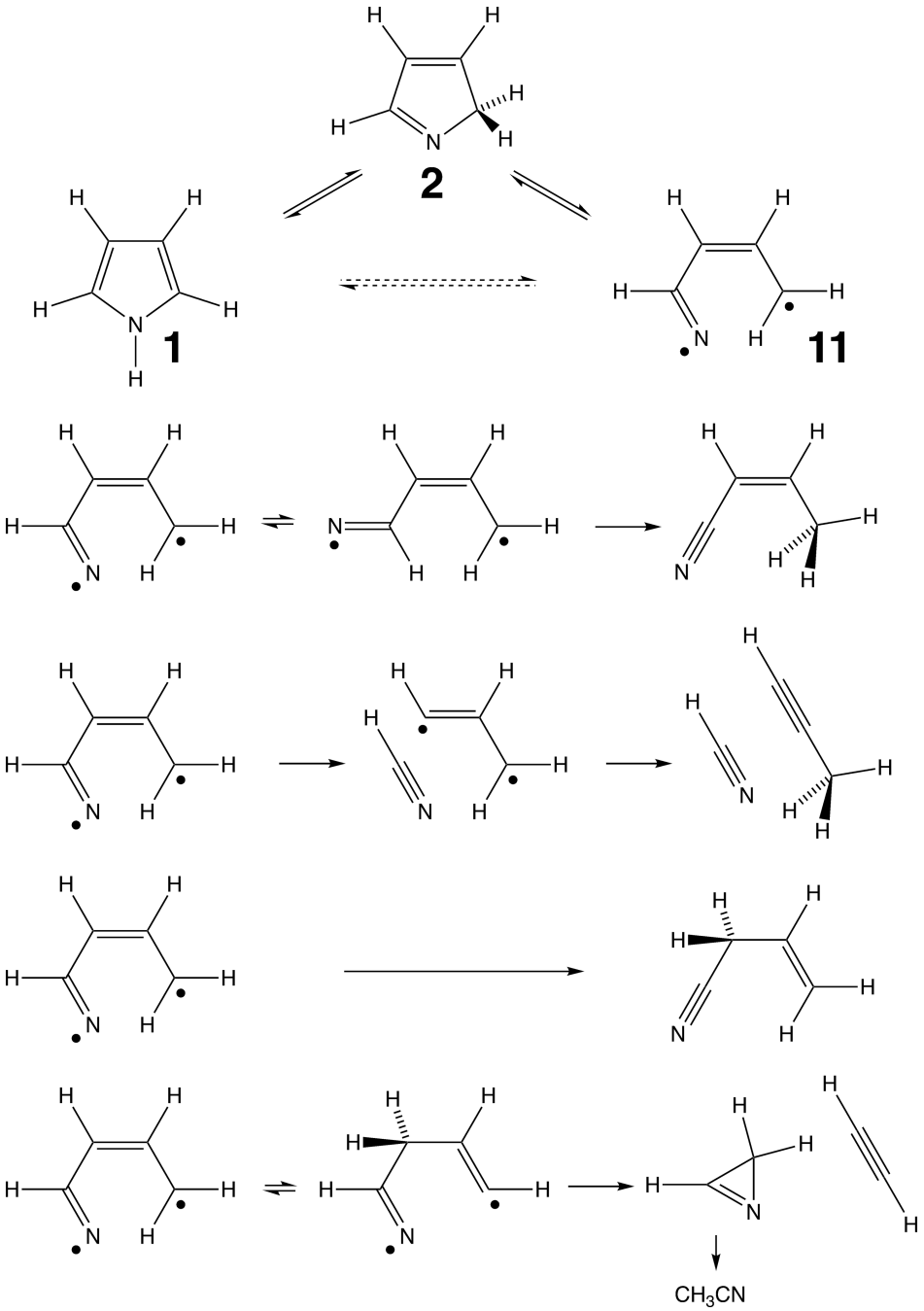

SCHEME 2 | Formation and subsequent reactions of the diradical **11**, suggested by the Lifshitz [2] and Mackie [3] groups.

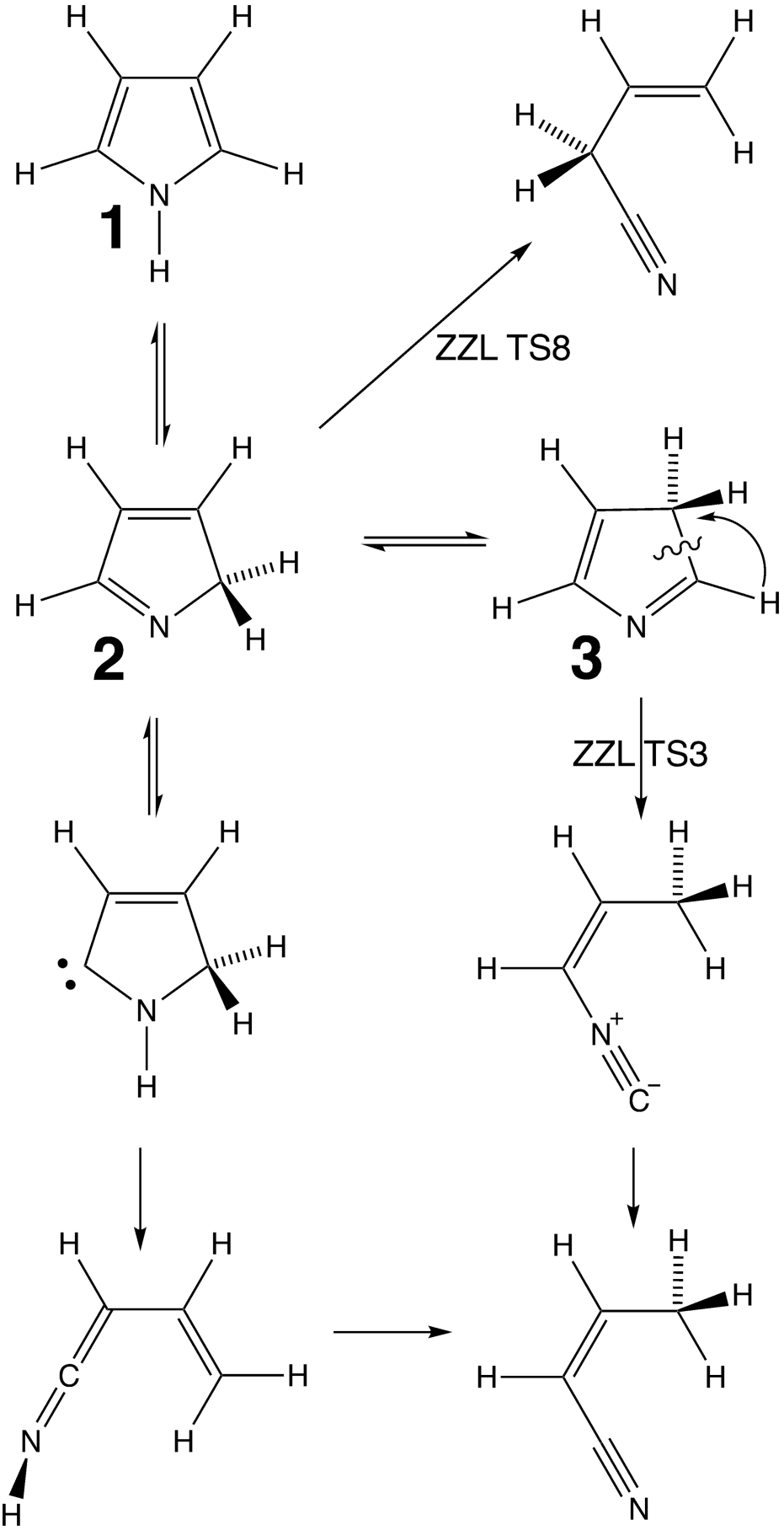

SCHEME 3 | Mechanistic proposals for formation of butenenitrile isomers from pyrrole by ZZL (ZZL) [7].

(Scheme 2), which they proposed to be directly formed from pyrrole, **1**, by a poorly precedented concerted C–N bond scission and H migration. Subsequently, Mackie et al. suggested a more plausible mechanism in which pyrrole first isomerized to 2*H*-pyrrole, **2**, and then ring opened to **11** [3].

The unorthodox numbering for the species arises from the desire to have a coherent numbering in later, more detailed schemes.

Several of the observed products could plausibly be derived from diradical **11**. The first three of its reactions, depicted in Scheme 2, were proposed by Lifshitz et al. [2], while the last one was proposed by Mackie and coworkers [3].

Dubnikova and Lifshitz (DL) [6] applied density functional theory (DFT) and ab initio wave function methods to study the formation of diradical **11** and its subsequent conversion to the butenenitrile isomers (i.e., the first and third of the diradical reactions in Scheme 2). In order to accommodate the necessarily multireference character of the wave function for singlet diradical **11** and its surrounding saddle points, DL used broken-symmetry UB3LYP. The geometries of the diradical species were checked with CASSCF(4,4) calculations. Both DFT and CASSCF calculations used the cc-pVDZ basis set. In an effort to refine the energetics, QCISD(T)/cc-pVDZ single point calculations were applied to the stationary point structures found at the lower levels. These results were checked by Zhai, Zhou, and Liu (ZZL) [7] in a paper published shortly after that by DL. Disturbingly, despite using identical theoretical methods, ZZL could not reproduce the results from DL [7]. Although structures and energies at the lower-level theory agreed, the higher-level single-point calculations disagreed by as much as 5.8 kcal/mol for identical structures. It is difficult to know what to make of this discrepancy, but at the very least it suggests that there is room for further theoretical work.

In general, ZZL disfavored diradical **11** as a significant intermediate in the formation of the observed products from pyrrole pyrolysis. They considered two alternative mechanisms for formation of (Z)-but-2-enenitrile, shown in Scheme 3.

Of the two pathways, their calculations favored the one via the isonitrile because the formation of the carbene in the alternative pathway was found to have too high a barrier. The ring opening to the isonitrile in the ZZL mechanism involves a concerted C–C cleavage and hydrogen migration, which is poorly precedented. Nevertheless, they reported finding a saddle point for it (ZZL TS3 in Scheme 3), with a structure that will be discussed in detail below.

ZZL also reported finding an energetically accessible saddle point (ZZL TS8 in Scheme 3) for concerted conversion of 2*H*-pyrrole to but-3-enenitrile. Its structure, too, will be discussed in detail below.

The fragmentation of diradical **11** to HCN and •HC = CH–CH_2•, proposed by DL (second diradical reaction in Scheme 2) was investigated by ZZL. They found its saddle point to be 110.3 kcal/mol above pyrrole, ruling it out as a viable pathway. ZZL were unable to locate any mechanism for HCN formation that would be energetically viable.

The most comprehensive mechanistic evaluation to date has been carried out by Martoprawiro, Bacskay, and Mackie (MBM) [8]. These authors investigated several new pathways from

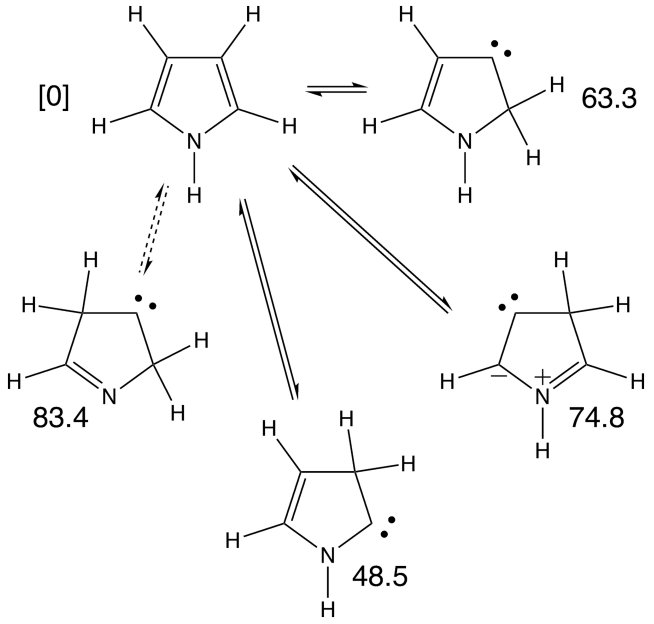

SCHEME 4 | Carbene isomers of pyrrole identified by MBM [8]. Numbers by each structure are their G2(MP2) relative heats of formation at 0 K, in kcal/mol.

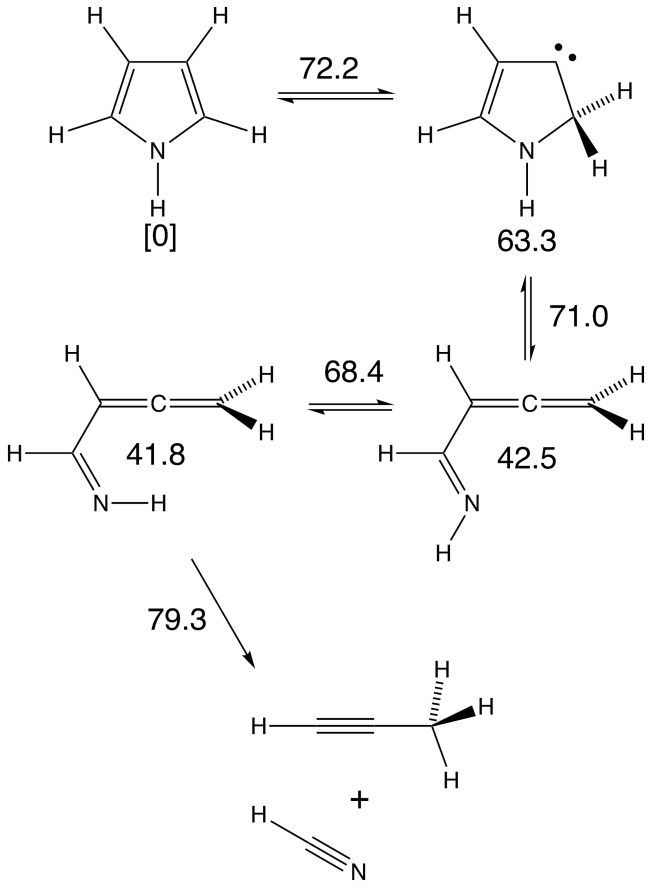

SCHEME 5 | Proposed mechanism for HCN formation from pyrrole. Numbers are MBM's relative enthalpies in kcal/mol at 0 K from their G2(MP2) calculations [8].

pyrrole to the observed products, but some of them were not energetically viable and so are not included here. MBM used CASSCF and CASPT2 calculations on diradical species and the composite G2(MP2) method for species reasonably represented by single-determinant wave functions. Their highest-level calculations on the diradicals were CASPT2/VTZ2P, where the basis-set designation VTZ2P signifies cc-pVTZ from which 4f functions on the heavy atoms and 3d functions on the hydrogens have been removed. They were single point calculations applied to the CASSCF/cc-pVDZ optimized structures.

A key feature of the MBM mechanism was the identification of four new carbene intermediates, derived by hydrogen migration from pyrrole. They are shown in Scheme 4. None of them correspond to the carbene proposed by ZZL and shown in Scheme 3.

One of these carbenes offered something that ZZL had been unable to find: an energetically viable route to the formation of HCN [9]. Their mechanism is shown in Scheme 5. One can see that the highest barrier was found to be that for the final retro-ene reaction, at 79.3 kcal/mol above pyrrole.

The reactions of Scheme 2 were subjected to CASPT2/cc-pVDZ analysis by MBM. The two fragmentation reactions of Scheme 2 were not reported, presumably because they were found to face insurmountable barriers. However, the other two reactions leading to the butenenitrile isomers were studied, with results

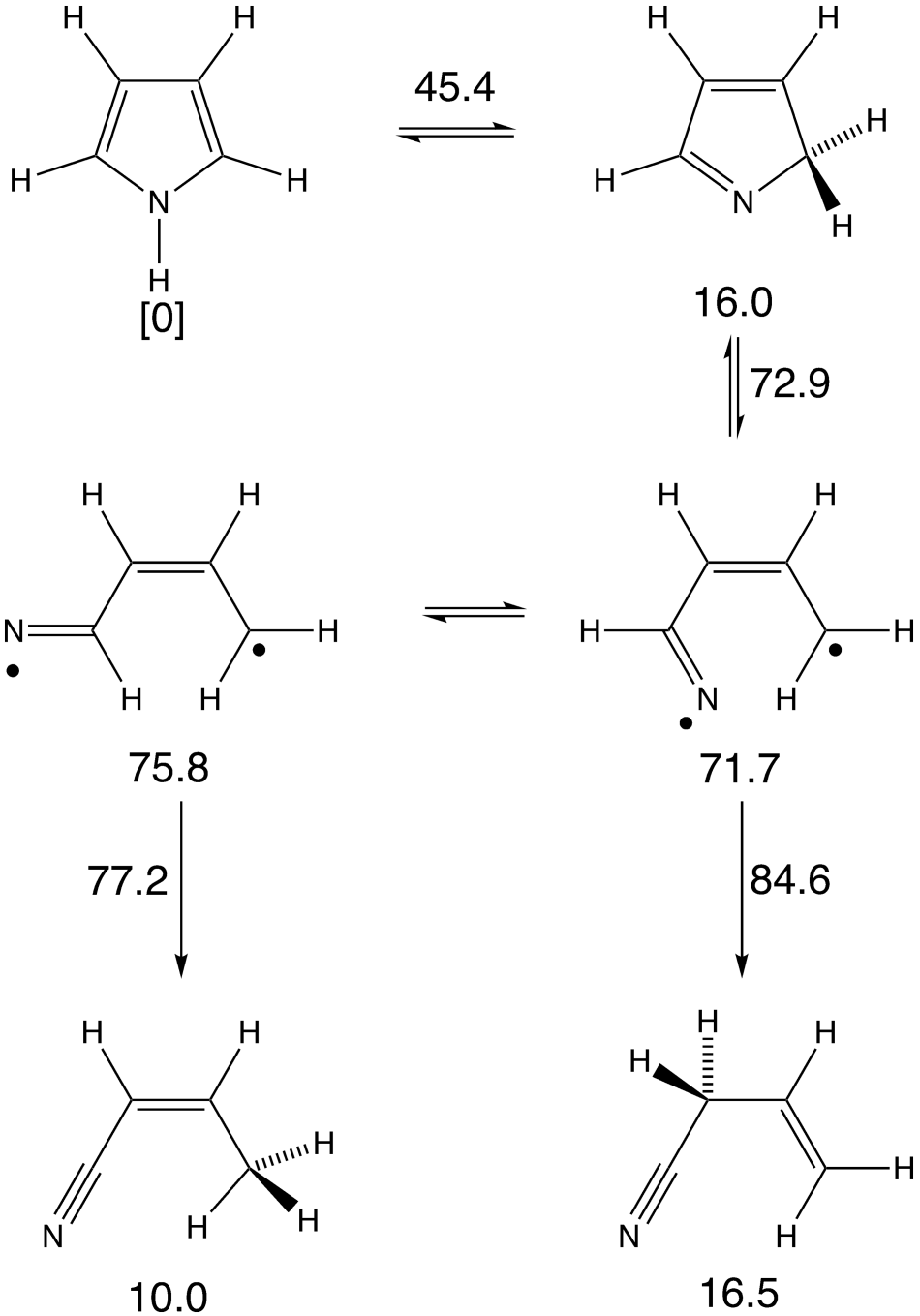

SCHEME 6 | CASPT2/cc-pVDZ relative enthalpies at 0 K, in kcal/mol from the calculations of MBM [8].

summarized in Scheme 6. Apparently, no saddle point was located for the internal rotation of diradical **11**. The competition between formation of the isomers was found to favor (*Z*)-but-2-enenitrile over but-3-enenitrile. Comparison with Scheme 5, would suggest formation of propyne + HCN to be competitive with both, as observed experimentally.

MBM did not discuss in detail mechanisms for the formation of acetylene, but as noted above, their experiments found it to be only a minor product at < 1400 K, in disagreement with Lifshitz et al. In their 117-step mechanism for the overall pyrolysis of pyrrole, MBM did have seven steps that would produce acetylene. Of these, the ones of largest rate constant corresponded to free-radical reactions. The free radicals, in their mechanism, would be initiated primarily by C–H homolysis of but-3-enenitrile via a saddle point that they calculated to be at least 95 kcal/mol above pyrrole [8]. This high barrier makes radical formation negligible below 1400 K.

2.3 | Possible Formation of Pyrrole From Allyl + •CN in Extraterrestrial Environments

Much recent attention has been paid to the detection of polyatomic molecules in extraterrestrial environments, such as the interstellar medium (ISM) [10], protoplanetary disks [11], and planetary atmospheres [12]. Of particular interest are molecules that, on Earth, are associated with life. Included in these are nitrogen heterocycles [13], such as pyrrole [14].

In general, it is believed that polyatomic molecule formation in the ISM occurs in two different phases. One is in the gas phase in cold molecular clouds, where reactions of resonantly stabilized radicals are believed to be of particular importance [15, 16]. The other phase is on the surface of dust particles or ice grains. A mechanism for pyrrole formation in the latter phase, with energy for reaction being supplied by cosmic rays, has been suggested, but so far, no gas-phase mechanism has been proposed [14].

Part of the purpose of the present work was to explore whether the reaction of allyl radical and •CN at low temperature and pressure could lead to pyrrole formation. Pyrrole has the lowest heat of formation of any species on the C_4H_5N potential energy surface, meaning that it could be the thermodynamic sink at low temperature. Furthermore, the reactant radicals have a combined heat of formation of 147.38 kcal/mol at 0 K [17]. This places them at 30–40 kcal/mol above most of the reaction barriers calculated by MBM, meaning that, in principle, all the reactions of pyrrole pyrolysis could be in play, with the energy being supplied by chemical activation rather than external heat.

In order to analyze the chemically activated reactions arising from allyl + •CN, one cannot rely on solving kinetic networks involving rate constants for the high-pressure limit, as has typically been done for pyrrole pyrolysis. Instead, one needs to solve a multiwell master equation. This latter model is equally appropriate for the radical-radical reaction at low temperature and pressure or for pyrrole pyrolysis at high temperature and pressure.

The purpose of the present work, then, has been to re-evaluate the mechanisms of pyrrole pyrolysis using higher level methods of electronic structure theory than have been employed to date. From the resulting network of species, a multiwell master equation has been used to simulate the kinetics. Finally, with exactly the same model, adjusted only to reflect different temperature, pressure, and initial concentrations, the viability of pyrrole formation from allyl + •CN has been assessed.

3 | Computational Methodology

As all the previous researchers of pyrrole pyrolysis have recognized, the network of intermediates on the C_4H_5N potential energy surface consists of many stationary points for which single-reference wave function methods are likely to be appropriate, but several more for which they are not. It is principally the singlet-state diradicals and their associated saddle points that fall into the latter class.

It is conventional in calculations involving thermally generated singlet diradicals to ignore the contributions of the corresponding triplet states on the grounds that, for hydrocarbons at least, the rate constants for reaction of the singlet states are typically orders of magnitude greater than their intersystem crossing (ISC) rate constants. However, much less is known about ISC in nitrogen-containing diradicals. Fortunately, a recent study suggests that for these species, too, ISC is quite slow and so unlikely to compete with reaction of the singlet states [18].

For the single-reference calculations, a modified version of the correlation-consistent composite approach (ccCA) of De Yonker, Cundari, and Wilson has been used [19]. This method was selected because it avoids the "high-level corrections" (HLCs) that the Gn and CBS methods employ. These HLCs have evolved to become adjustable parameters that improve the fit to experimental heats of formation for molecular species in predefined test sets. However, all the experimental data are for species existing as local minima on their respective potential energy surfaces. It is therefore an act of faith that the same HLCs will apply to calculations on saddle points. By eschewing HLCs altogether, the various ccCA methods avoid this problem [20].

The ccCA method used in the present work is based on ccCA-aTZ-QCISD(T), which uses the B3LYP density functional for geometry optimization and zero-point energy (ZPE) calculations. It then performs the following single-point calculations:

$$E_{\mathrm{Ref}} = E\,(\mathrm{QCISD(T)}\,/\,\mathrm{aug-cc-pVTZ})$$

$$E_{\mathrm{MP2Small}} = E\,(\mathrm{MP2}\,/\,\mathrm{aug-cc-pVTZ})$$

$$E_{\mathrm{MP2Big}} = E\,(\mathrm{MP2}\,/\,\mathrm{aug-cc-pVQZ})$$

$$\Delta E_{\mathrm{pol}} = E_{\mathrm{MP2Big}} - E_{\mathrm{MP2Small}}$$

$$E_{\mathrm{MP2Full}} = E((\mathrm{MP2,full})\,/\,\mathrm{aug-cc-pCVTZ})$$

$$\Delta E_{\mathrm{CV}} = E_{\mathrm{MP2Full}} - E_{\mathrm{MP2Small}}$$

$$E_{\mathrm{final}} = E_{\mathrm{Ref}} + \Delta E_{\mathrm{pol}} + \Delta E_{\mathrm{CV}} + \mathrm{ZPE}_{\mathrm{Scaled}}$$

The modification for the present work is that geometry optimizations and ZPE calculations were carried out at the M062X/cc-pVTZ level, with a scale factor of 0.98525 being applied to the calculated ZPEs. The reason for this choice is that it has been shown that M062X performs better than B3LYP on reaction saddle points [21].

The applicability of the ccCA model was evaluated by calculation of the T_1 diagnostic during the QCISD(T) step. In accord with convention [22], values of T_1 below 0.02 were deemed to indicate that a single-reference wave function was appropriate.

When the QCISD(T) T_1 value exceeded 0.02, a multireference electronic structure model was adopted. This approach was based on CASSCF/cc-pVTZ geometry optimization and intrinsic reaction coordinate (IRC) calculation, with the active space being different for different reactions, but consistent throughout the IRC from reactant through saddle point to product(s). In order to correct the CASSCF wavefunctions for dynamic correlation, single-point NEVPT2-F12/cc-pVTZ-F12 calculations were carried out [23]. However, these were not simply evaluated at the CASSCF saddle-point geometries. Instead, several points along the CASSCF IRC were calculated and then interpolated with a cubic spline, in an effort to approach the true NEVPT2-F12 saddle-point energy. The F12 explicit correlation provides a way to get closer to the complete-basis-set energy in a cost-effective manner [23].

Electronic-structure calculations used the ORCA (Version 6.1) [24] and GAMESS-US (Version 15 JUL 2024 (R2 Patch 1)) [25, 26] software packages.

For the master-equation calculations, the Arkane [27] program was employed. This takes as input the 0 K enthalpies, moments of inertia, vibrational frequencies, and collisional parameters for each stationary point. In addition, when the structure includes internal rotors, hindered-rotor partition functions are evaluated. This step requires information about the internal rotation potential energy profiles for each rotor. These were evaluated at the M062X/cc-pVTZ level.

4 | Results and Discussion

4.1 | Analysis of the Novel Mechanisms of ZZL

As outlined in the Introduction, ZZL [7] disfavored the intermediacy of diradical **11** in pyrrole pyrolysis, but instead proposed two novel mechanisms, characterized by the saddle points ZZL TS3 and ZZL TS8 in Scheme 3. The ZZL paper did not provide Cartesian coordinates for these saddle points, but from the reported structural parameters and relative energies, it has been possible to recalculate them. The results are shown in Figures 1 and 2.

Aside from the two angles highlighted in red in Figure 1, all geometrical parameters for ZZL TS3 agree to ±0.001 Å or ±0.1° with those reported by the authors. The relative energies and zero-point energies are also identical.

The recalculated structure for ZZL TS8 is quite problematic. It seems clear from the very close similarity in geometrical parameters and energies that the original and recalculated structures are identical. However, the depiction of the methylene hydrogens by ZZL is misleading. Their wedge and dash representation clearly implies that the two hydrogens are above and below the average plane of the carbon atoms. However, the recalculated structure shows that they are very close to being in that plane, as indicated, for example, by the highlighted dihedral angle.

Although distances from the methylene hydrogens to the nitrogen are not reported by ZZL, one would certainly expect from their depiction that both would be at least as far away from the nitrogen as the carbon to which they are attached is. In reality, as shown in Figure 2, one of the methylene hydrogens is much closer to the nitrogen than the carbon to which it is attached.

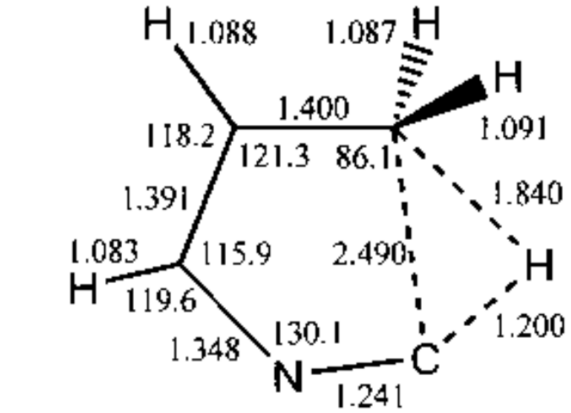

ZZL TS3: E_{rel} = 85.1; ZPE = 46.8

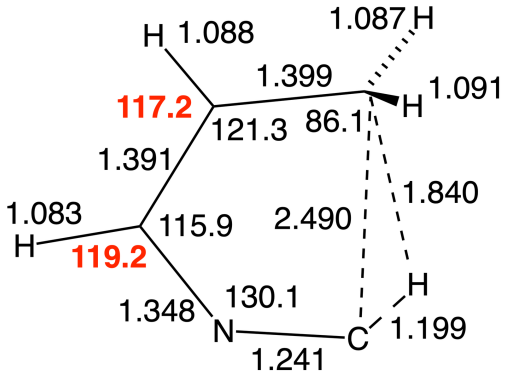

This work: E_{rel} = 85.1; ZPE = 46.8

FIGURE 1 | Recalculation of the saddle point ZZL TS3 at the B3LYP/6-31G(d.p) level used by the authors [7]. Relative energies are in kcal/mol with respect to pyrrole. Original structure from ZZL reprinted with permission from the American Chemical Society.

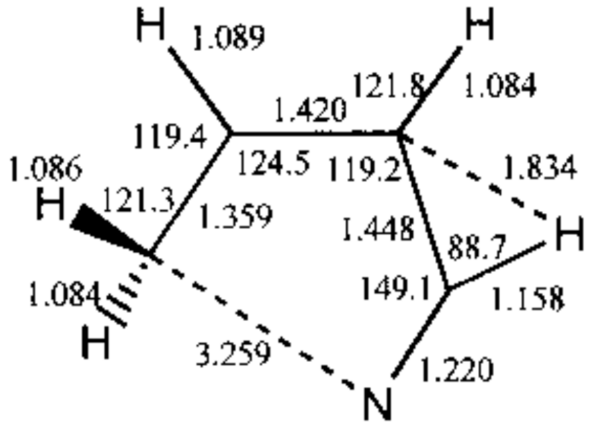

ZZL TS8: E_{rel} = 94.4; ZPE = 46.3

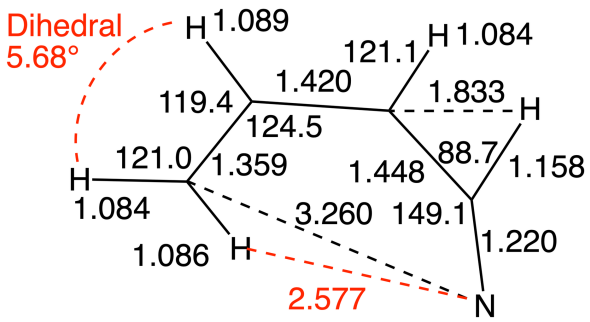

This work: E_{rel} = 94.4; ZPE = 46.3

FIGURE 2 | Recalculation of the saddle point ZZL TS8 at the B3LYP/6-31G(d.p) level used by the authors [7]. Relative energies are in kcal/mol with respect to pyrrole. Original structure from ZZL reprinted with permission from the American Chemical Society.

Further calculations on ZZL TS3 and TS8 appear to invalidate the mechanisms for which they are purported to be transition states. As shown in Scheme 3, ZZL TS3 is supposed to connect 3*H*-pyrrole to an acyclic isonitrile. However, when one runs an IRC calculation from this saddle point that is not what one finds (Figure 3). Instead of connecting to 3*H*-pyrrole, their TS3 connects to structure **4**. Interestingly, this structure had been identified as an intermediate by MBM [8], but they did not consider the possibility of its connecting to the isonitrile. Instead, they investigated a seemingly higher barrier pathway for its fragmentation to propyne and HCN. Thus, it appears that ZZL did indeed find a new mechanistic pathway; it just was not the one they thought it was.

In principle, one could similarly conduct an IRC calculation starting from ZZL TS8. However, this structure has another problem, which makes such an exercise pointless. If one carries out a stability test on the Kohn-Sham wave function from the B3LYP calculations, one finds that it has an RDFT → UDFT instability. This means that the calculation is invalid and that the molecular structure is not a true stationary point on the potential energy surface.

From these calculations, one must consequently conclude that neither of the novel mechanisms favored by ZZL is valid.

4.2 | Examples of the NEVPT2-F12 Calculations

As described in the section on computational methodology, the NEVPT2-F12 calculations were somewhat more involved than simple single-point calculations at the CASSCF stationary points. The procedure can be illustrated with the hydrogen migration that converts diradical **11** to (Z)-but-2-enenitrile, as illustrated in Scheme 6. Figure 4 shows the CASSCF(8,8)/cc-pVTZ IRC for the reaction. It is the solid blue line. The red dots indicate NEVPT2-F12(8,8)/cc-pVTZ-F12 single-point calculations carried out at regular intervals along the CASSCF IRC. The green line is a cubic spline interpolating between the red points.

The first thing to notice is that one end of the IRC corresponds to a structure not considered in any of the previous calculations on pyrrole pyrolysis, namely 2-vinyl-2*H*-azirine. Secondly, one sees that the singlet diradical is not found to be a local minimum in these calculations. Instead, it sits on an extended energy plateau, as is commonly the case for singlet diradicals. In fact, there are two such plateaus, each corresponding to a reaction-path bifurcation. In the region labeled **B** in Figure 4, there is an internal rotation of the C–C bond to the terminal methylene. However, there are two senses in which this rotation can occur, interchanging *E* and *Z* hydrogen locations for the methylene hydrogens, once they are in the carbon plane. The second bifurcation occurs when the •N = C–H moiety rotates out of the plane prior to forming the azirine ring. Again, there are two senses with which this can occur, leading to the two enantiomers of the 2-vinyl-2*H*-azirine. By construction, the saddle point for the CASSCF occurs exactly at 0 on the reaction coordinate axis. However, the maximum along the NEVPT2-F12 curve does not. It is quite far removed from zero. In fact, differentiation of the spline interpolation function locates it at −2.13 $\sqrt{\text{amu•bohr}}$. Had one just done a single point NEVPT2-F12 calculation at the CASSCF saddle point, one would have underestimated the energy of the saddle point by several kcal/mol.

Figure 5 shows analogous plots for the IRC connecting 2-vinyl-2*H*-azirine to but-3-enenitrile. Again, the diradical **11** appears only as a plateau, not as a distinct intermediate. This time, the NEVPT2-F12 and CASSCF saddle points are much closer to each other in energy and in position along the reaction coordinate.

The NEVPT2-F12 calculations make the barriers to formation of the butenenitrile isomers almost identical. This contrasts with MBM's CASPT2 calculations, which found a 7.4 kcal/mol preference for formation of (*Z*)-2-butenenitrile (Scheme 6). The difference in results can be traced largely to the change in saddle point position along the reaction coordinate between CASSCF and multireference PT2 calculations, as described above.

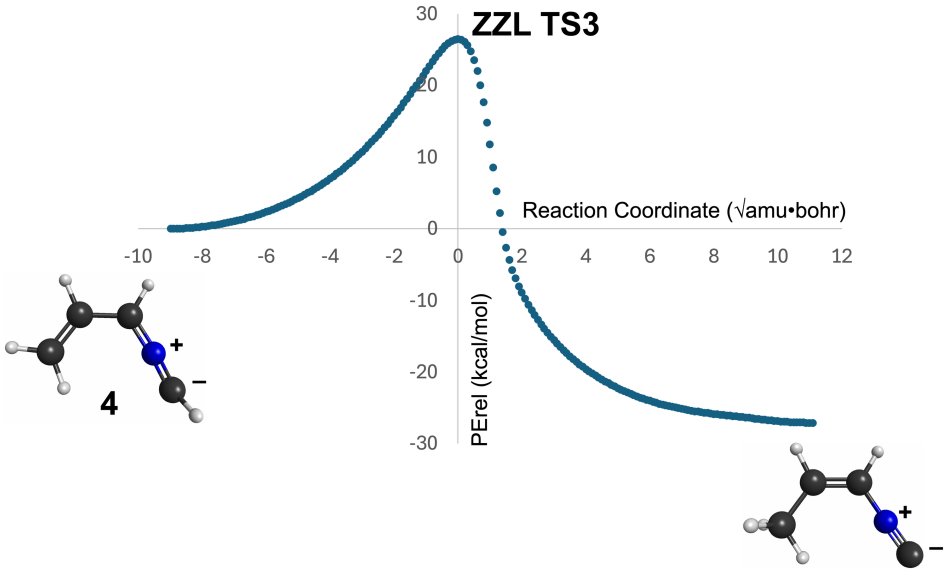

FIGURE 3 | B3LYP/6-31G(d,p) IRC showing the connectivity of ZZL TS3.

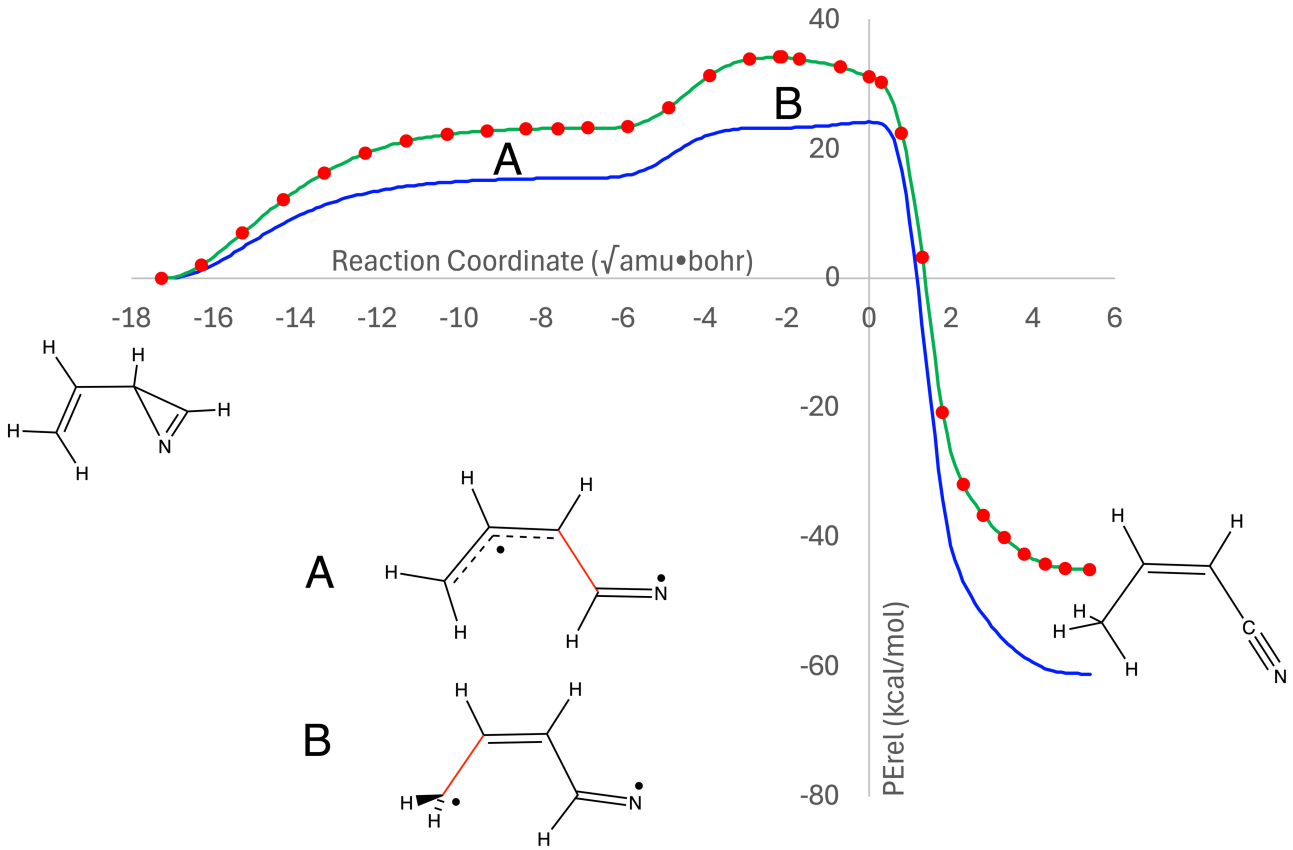

FIGURE 4 | CASSCF(8,8)/cc-pVTZ and NEVPT2-F12(8,8)/cc-pVTZ-F12 calculations for the conversion of 2-vinyl-2*H*-azirine to (*Z*)-but-2-enenitrile. The blue line is the CASSCF IRC. The red dots are single-point NEVPT2-F12 calculations carried out along the CASSCF IRC. The green line is a cubic spline interpolation between the red points.

Of course, one wants to know how the diradical **11** connects also to 2*H*-pyrrole, because that is the principal reaction, which connects everything else to the pyrrole reactant in the MBM mechanism. The answer, according to the present work, is shown in Figure 6. At the CASSCF level, the diradical faces a PE barrier of 2.47 kcal/mol. However, the NEVPT2-F12 picture is again different. If finds a saddle point at a reaction coordinate of 0.214 √amu•bohr and a PE of only 0.60 kcal/mol. Once one includes zero-point energies for the stationary points, the barrier disappears altogether.

Thus, the picture that emerges from the NEVPT2-F12 calculations is that diradical **11** sits on a broad plateau with barrierless exits to both enantiomers of 2-vinyl-2*H*-azirine and to

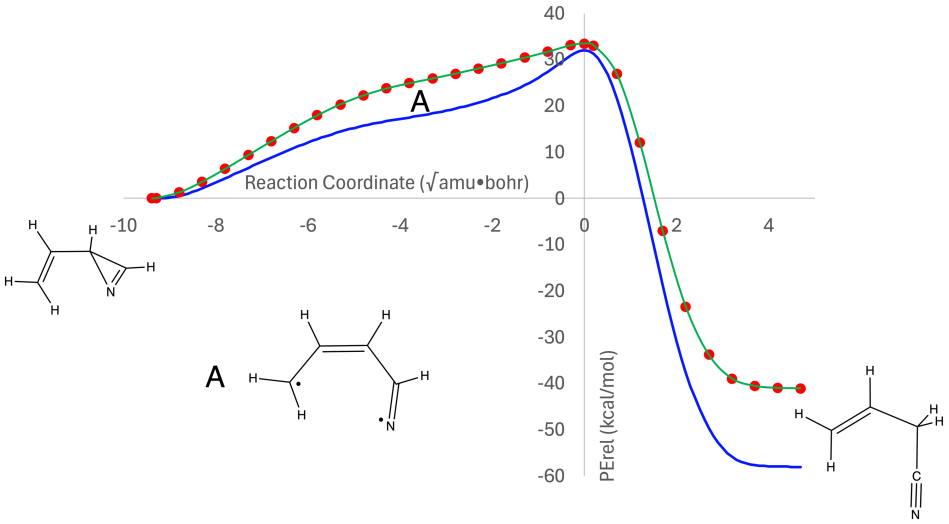

FIGURE 5 | CASSCF(8,8)/cc-pVTZ and NEVPT2-F12(8,8)/cc-pVTZ-F12 calculations for the conversion of 2-vinyl-2*H*-azirine to but-3-enenitrile. The blue line is the CASSCF IRC. The red dots are single-point NEVPT2-F12 calculations carried out along the CASSCF IRC. The green line is a cubic spline interpolation between the red points.

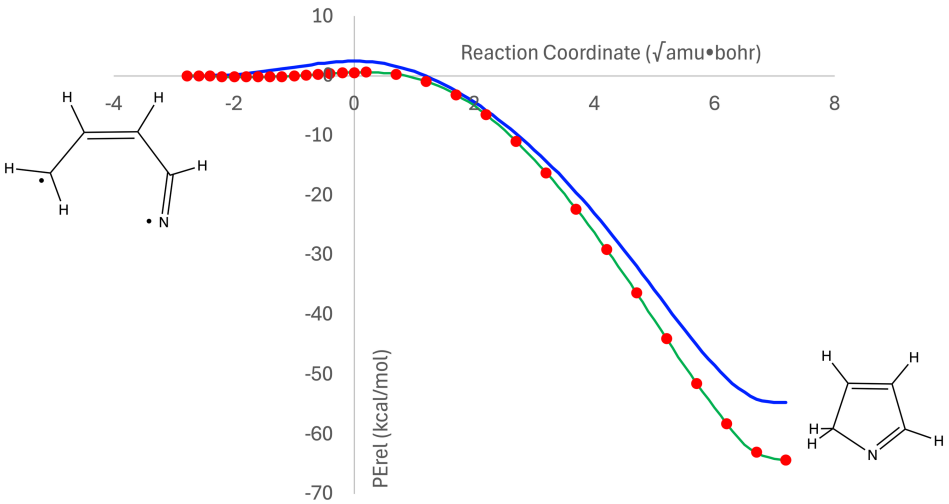

FIGURE 6 | CASSCF(10,9)/cc-pVTZ and NEVPT2-F12(10,9)/cc-pVTZ-F12 calculations for the ring closure of singlet diradical **11** to 2*H*-pyrrole. The blue line is the CASSCF IRC. The red dots are single-point NEVPT2-F12 calculations carried out along the CASSCF IRC. The green line is a cubic spline interpolation between the red points.

2*H*-pyrrole, but with barriers to formation of the butenenitrile isomers.

4.3 | Summary of the Stationary Points Found on the Potential Energy Surface for Pyrrole Pyrolysis

The modified ccCA single-reference and the NEVPT2-F12 multireference calculations have been combined to afford an overall mechanistic scheme for pyrrole pyrolysis. The Arkane [27] multiwell master equation program automatically generates an overall potential energy profile for all species, and it is included with the Supporting Information for the sake of completeness but, frankly, it is more or less incomprehensible because it is so complex. Instead, the mechanism is summarized here as a series of schemes showing formation of the key products. In each scheme, the floating-point number under each structure is its calculated heat of formation at 0 K, reported in kcal/mol. The numbers above each arrow are the heats of formation for the saddle points. One minor point merits discussion. All experiments on pyrrole pyrolysis have found that both (*E*)- and (*Z*)-isomers of but-2-enenitrile are formed. All prior researchers have assumed that the two isomers interconvert under the reaction conditions, and calculations by MBM supported this picture [8]. Because the two isomers are essentially isoenergetic (0 K heats of formation of 38.82 and 38.46 kcal/mol, respectively according to the present calculations), the *E*–*Z* isomerization has not been included in the mechanism. Instead, the (*Z*)-isomer is taken as a surrogate for the equilibrium mixture.

A few remarks are perhaps in order about the mechanistic schemes. In Scheme 7, one sees the product **6**, connected in single steps to intermediates **12** and **31**.

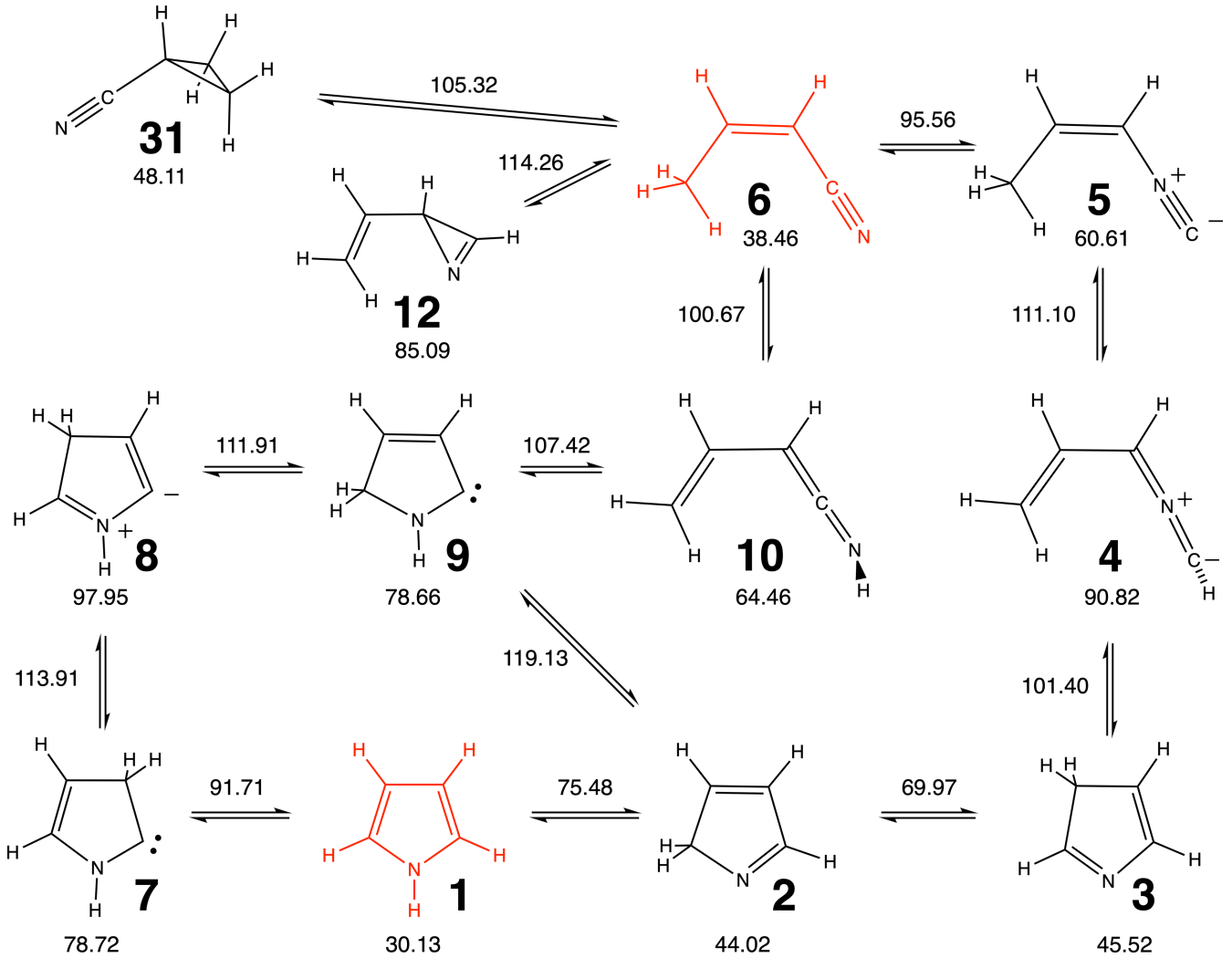

SCHEME 7 | Mechanistic pathways from pyrrole (**1**) to (*Z*)-but-2-enenitrile (**6**). Floating-point numbers under each structure are calculated heats of formation at 0 K in kcal/mol. Those above each arrow are calculated heats of formation at 0 K for the corresponding saddle points.

The connection to **12** was shown in more detail in Figure 3. It occurs via diradical **11**, but because this is not an intermediate, it is not shown explicitly. Similarly, the connection of **6** to cyanocyclopropane, **31**, occurs via a singlet diradical—1-cyanotrimethylene—but again the calculations do not find it to be a local minimum on the potential energy surface. MBM found the same thing in their calculations.

Also in Scheme 7, one sees direct conversion of 2*H*-pyrrole, **2**, to carbene **9**. It faces a significant barrier. ZZL found the same connection in their calculations and also computed a substantial barrier. For this reason, they ruled the reaction out. What they did not find is the alternative indirect connection of **2**–**9** via intermediates **7** and **8**. Intermediate **8** is a new addition to the mechanism of pyrrole pyrolysis, not having appeared in any of the prior mechanistic schemes. The indirect conversion of **2**–**9** faces a maximum barrier that is 5.2 kcal/mol below that for the direct reaction.

The ring opening of 3*H*-pyrrole to intermediate **4** was identified by MBM. However, as discussed above, they did not find the connection between intermediates **4** and **5**. The saddle point for the conversion of **4**–**5** is the one that ZZL had thought directly connected **3** and **5** (ZZL TS3).

In Scheme 8, diradical **11** is shown explicitly, but it is placed in brackets. The meaning here is that the CASSCF calculations on ring opening of 2*H*-pyrrole, **2**, did find a shallow local minimum for this diradical. However, the addition of the NEVPT2-F12 correlation correction and ZPE terms made that minimum disappear. Hence, as discussed above, the diradical is best thought of as sitting on an energy plateau with some barrierless exits (to **2** and **12**) and some reactions facing small barriers (to **6**, **10**, and **13**). Allyl radical (**15**) and •CN (**16**) are shown in Scheme 8 not because they play any significant role in pyrrole pyrolysis, but rather to show how these species connect into the whole mechanistic network once the calculations relevant to reactions in the ISM are undertaken.

4.4 | Master Equation Analysis of the Mechanism for Pyrrole Pyrolysis

The complete mechanistic scheme outlined above was subjected to master equation analysis at pressures from 0.1 to 100 bar and temperatures from 1000 to 1400 K. Both helium and argon bath gasses were examined. The Arkane software provides solutions to the master equation problem in

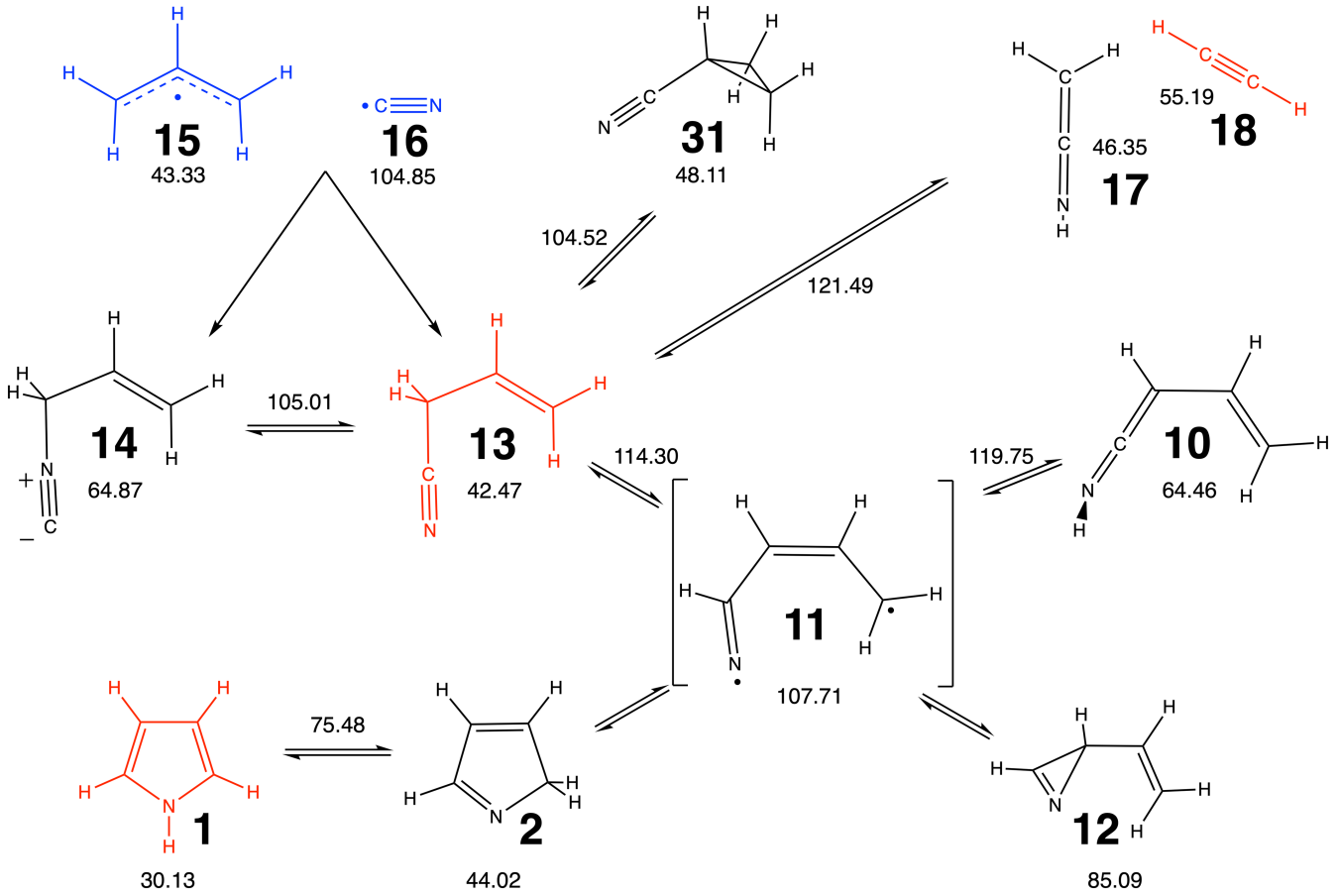

SCHEME 8 | Mechanistic pathways from pyrrole (**1**) to but-3-enenitrile (**13**) and acetylene (**18**). Floating-point numbers under each structure are calculated heats of formation at 0 K in kcal/mol. Those above each arrow are calculated heats of formation at 0 K for the corresponding saddle points.

terms of Chebyshev polynomials in two variables (temperature and pressure). The polynomials afford interpolations for each $k_{ij}(T,P)$, which are the effective rate constants connecting species i to species j in the mechanistic network. Together, this set of rate constants, along with a set of specified initial concentrations for the species, can be integrated to provide the time-dependent concentration of each intermediate at the chosen temperature and pressure. In the present work, the equations were integrated with the Python module scipy.integrate.odeint, which switches automatically between the Adams method for nonstiff equations and the backward differentiation formula for stiff equations.

The results were found to be essentially independent of pressure above 5 bar and also showed very little dependence on the nature of the bath gas at these pressures. These high-pressure-limit results were taken to be representative of the shock tube conditions. A typical result for 1350 K and 10 bar is shown in Figure 7.

As outlined in the introduction, both the Lifshitz and Mackie groups reported effective Arrhenius expressions for the disappearance of pyrrole in their shock-tube studies. Lifshitz et al. also gave effective Arrhenius expressions for the appearance of several of the products. In order to do so, they evaluated the quantity $\log_{10}((1/t)[\text{product}]/[\text{pyrrole}]_0)$ and plotted it against reciprocal temperature. Such a plot presumes that the product formation is first order. Then, even if it is, the expression is valid only at values of the time, t, corresponding to low conversion. The authors do not specify either a time or a percent conversion at which their measurements were made, and so to compare the present results with their results, two different possibilities have been explored. One is to evaluate the expression for each product at a time of 2 ms, corresponding to the reported residence time after the reflected shock wave in the Lifshitz experiments, but meaning that the percent reaction will be different at each temperature. The other is to use a fixed 1% conversion, meaning that the time of evaluation is different for each temperature. The results are summarized in Table 1.

Several points need to be made about the results in Table 1. First, the uncertainties in the calculated activation energies and pre-exponential factors are obviously not due to experimental error. They are, instead, errors due to lack of fit of the model. The fact that they exist and are substantial reveals an important conclusion. The disappearance of pyrrole and the appearances of the various products are not first-order processes and so it is simply a mistake to try to fit them to Arrhenius expressions. Given that fact, it is not surprising that the different attempts to make them fit (taking data at constant time or constant percentage reaction) lead to different results, but the variation is certainly striking! Perhaps the estimates for pyrrole loss are reasonably robust and meaningfully compared with the experimental values, but it is difficult to conclude that the Arrhenius values for individual product

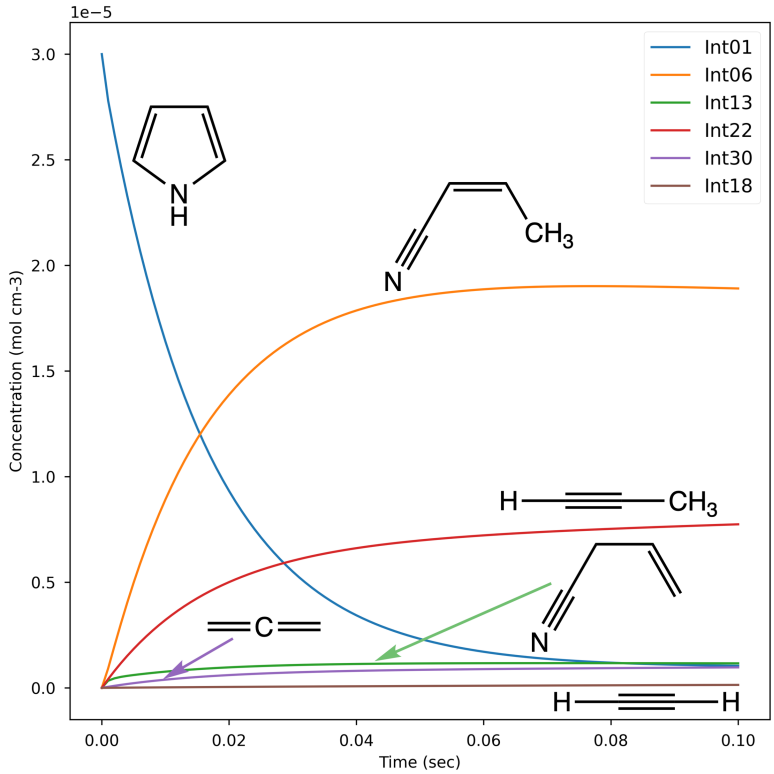

FIGURE 7 | Calculated time-dependent concentrations of key species at 1350 K and 10 bar.

TABLE 1 | Attempts to fit temperature dependent reactions to Arrhenius expressions and comparisons with experiment. Species key: **1** = pyrrole, **6** = but-2-enenitrile, **13** = but-3-enenitrile, **18** = acetylene, **23** = HCN. Activation energies are in kcal/mol and A factors in s^{-1}.

	2-ms reaction time		1% conversion		Experiment	
Species	E_a	$Log_{10}(A)$	E_a	$Log_{10}(A)$	E_a	$Log_{10}(A)$
1	78.28 ± 2.75	14.39 ± 0.51	78.46 ± 2.74	14.36 ± 0.51	75[a]	14.83[a]
					80[b]	15.90[b]
					74.1 ± 3.0[c]	14.1 ± 0.7[c]
6	82.63 ± 3.12	14.77 ± 0.58	77.24 ± 3.05	13.82 ± 0.57	72	14.02
13	68.56 ± 1.14	11.93 ± 0.21	83.50 ± 2.03	14.69 ± 0.38	77	14.60
18	90.72 ± 1.77	13.57 ± 0.33	80.99 ± 2.80	11.90 ± 0.52	77	14.28
23	75.67 ± 2.28	13.34 ± 0.42	76.56 ± 2.81	13.51 ± 0.48	84	15.80

[a]Lifshitz "initiation" values.
[b]Lifshitz "overall" values.
[c]Mackie values.

formation have much significance at all. The only thing one can meaningfully do is to look at qualitative ratios of products. The present simulation finds (Z)-but-2-enenitrile to be the principal product under most conditions studied, and that does seem to be in accord with experiment. Similarly, relatively high amounts of propyne, allene, HCN and but-3-enenitrile are in accord with the experimental results. The one striking difference between the present simulation and the Lifshitz results concerns the amount of acetylene produced. They saw much more than the simulation predicts. However, as noted previously, Mackie and coworkers saw acetylene appear in substantial amounts only above 1400 K, which is outside the temperature range of this work. Consequently, the present simulation seems to fit the Mackie results better than the Lifshitz results.

In order to explain the higher rate of disappearance of pyrrole and the appearance of unusual products, such as cyanoethane, in the Lifshitz experiments, Mackie and coworkers suggested that there may have been impurities in the Lifshitz samples. Any impurity that initiated a low-temperature chain reaction (with oxygen being an obvious candidate) would not only help to explain the difference between the Mackie and Lifshitz experiments; it would also explain why Lifshitz found different "initiation" and "overall" rates for disappearance of pyrrole, whereas Mackie et al. found only one rate.

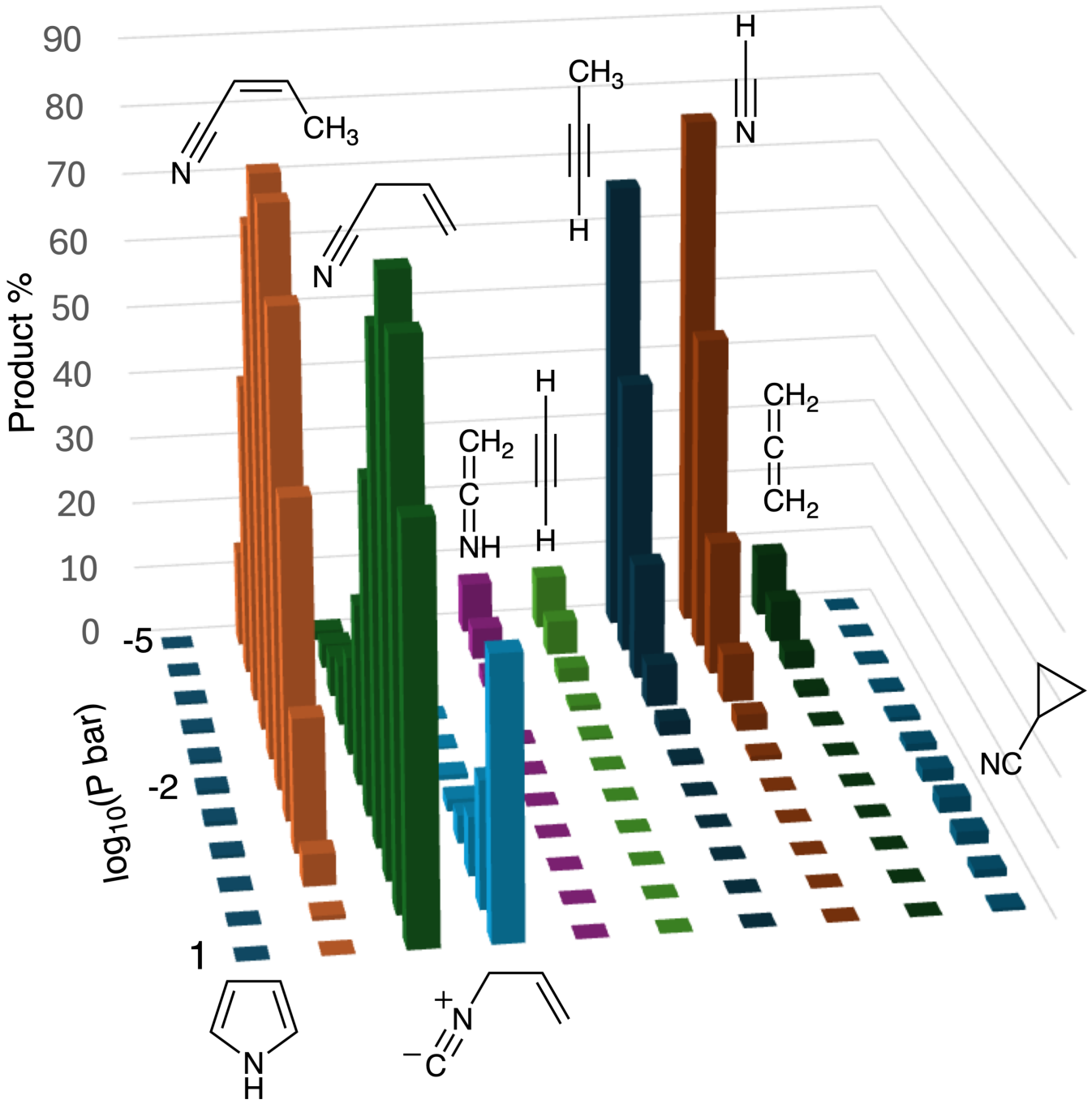

FIGURE 8 | Pressure dependence of product formation in the reaction of allyl radical with •CN. The vertical axis, labeled as "Product %" is actually the ratio of the concentration of each product to the initial concentration of allyl radical, expressed as a percentage.

4.5 | Master Equation Analysis for the Reaction of Allyl Radical With •CN

As outlined in the introduction, one of the purposes of the present work was to find out whether the reaction of allyl radical with •CN could provide an extraterrestrial route to the formation of pyrrole. Rather than relying on external heat to drive the reaction, one would now be looking for chemical activation, arising from the high exothermicity of the radical-radical reaction, to do the job.

In order to simulate this circumstance, the Arkane master equation package was run for a temperature of 150 K (which was the lowest temperature at which the software gave converged results) and pressures from 10^{-5} to 10 bar. The initial concentrations of the two reactants were set to 5.0×10^{-6} mol cm^{-3}. The results are summarized in Figure 8.

What one sees is that, at the lowest pressure, the principal products are the low molecular-weight gases HCN and propyne. There are also appreciable amounts of allene and even acetylene formed. This last product, constituting 7.8% of the initial concentration of allyl radical at 10^{-5} bar, seems somewhat surprising, given how little of it was produced in the simulation of pyrrole pyrolysis. There are two routes to acetylene in the present mechanism. They can be distinguished because

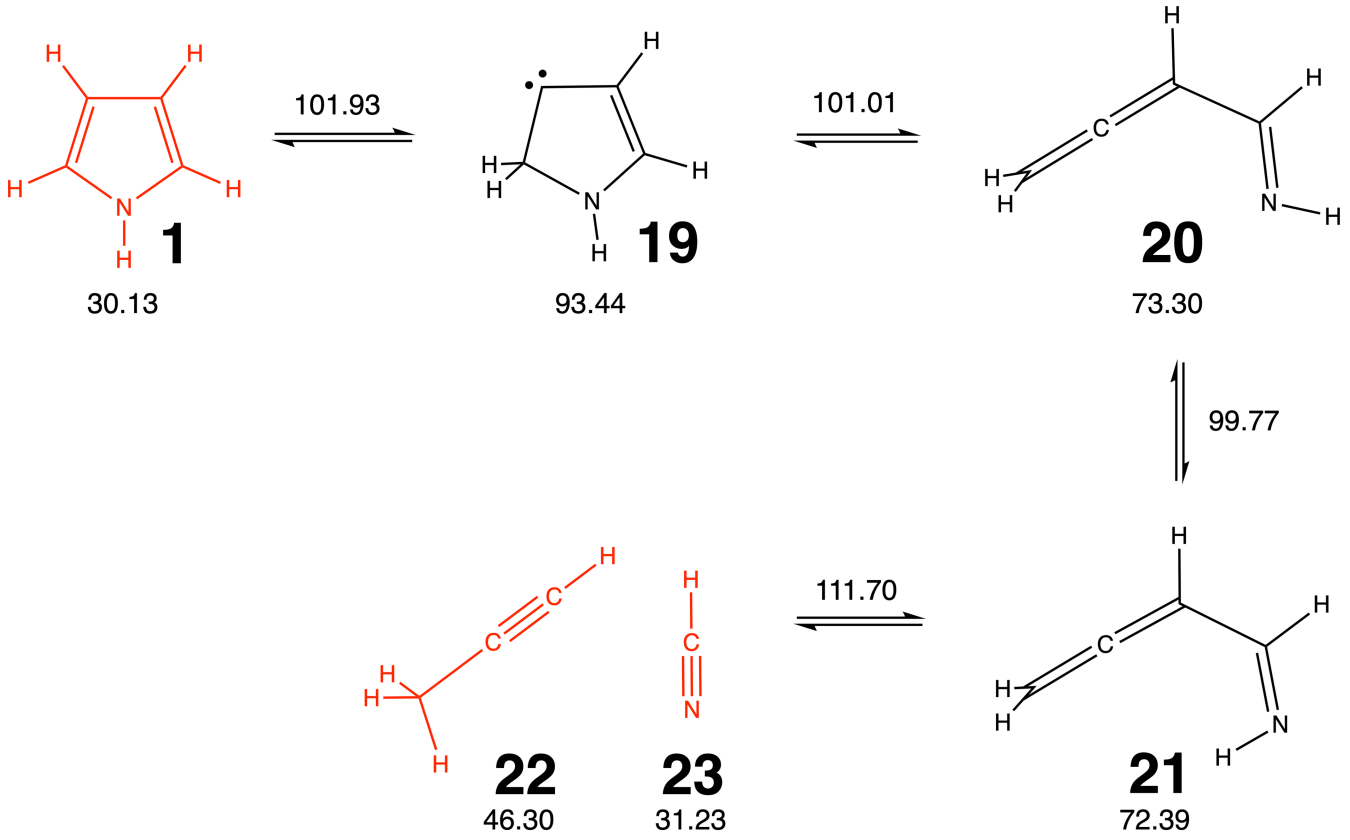

SCHEME 9 | Mechanistic pathway from pyrrole (**1**) to propyne (**22**) and HCN (**23**). Floating-point numbers under each structure are calculated heats of formation at 0 K in kcal/mol. Those above each arrow are calculated heats of formation at 0 K for the corresponding saddle points.

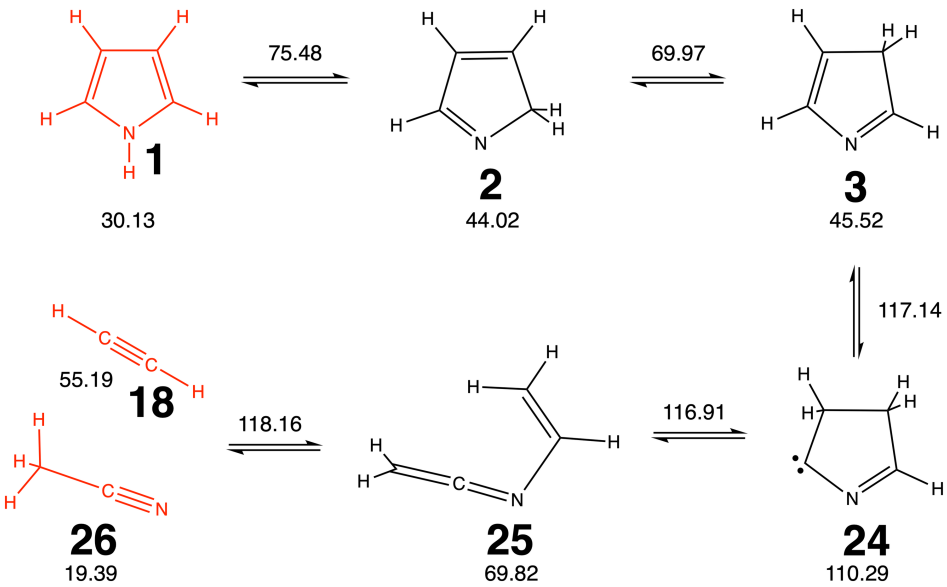

SCHEME 10 | Mechanistic pathway from pyrrole (**1**) to acetylene (**18**) and acetonitrile (**26**). Floating-point numbers under each structure are calculated heats of formation at 0 K in kcal/mol. Those above each arrow are calculated heats of formation at 0 K for the corresponding saddle points.

they produce different coproducts. One path (Schemes 8 and 9) produces ketenimine, **17**. The other (Schemes 10 and 11) produces acetonitrile, **26**. As can be seen in Figure 8, the outcome is unambiguous: 95% of the acetylene arises from the direct retro-ene reaction of but-3-enenitrile (Scheme 8), despite the fact that this reaction has a barrier that is 3.3 kcal/mol higher in 0 K enthalpy than the alternative. The reason, presumably, is that the retro-ene reaction is directly connected to the local "hot spot" generated by the radical combination, whereas the alternative mechanism occurs only after several intervening steps, during which the excess kinetic energy can be dissipated among many different species.

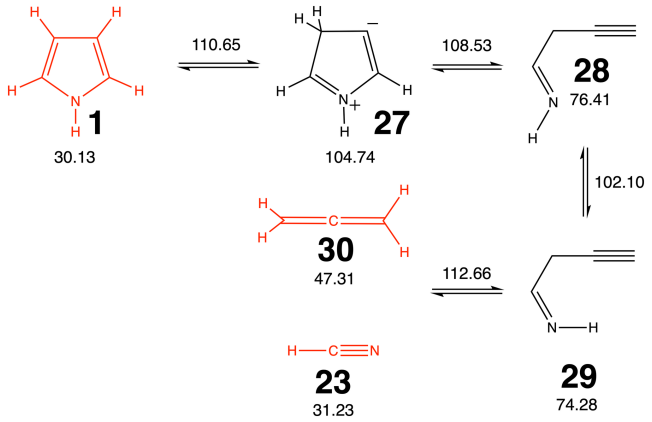

SCHEME 11 | Mechanistic pathway from pyrrole (**1**) to HCN (**23**) and allene (**30**). Floating-point numbers under each structure are calculated heats of formation at 0 K in kcal/mol. Those above each arrow are calculated heats of formation at 0 K for the corresponding saddle points.

As the pressure is increased, the HCN and propyne production decreases and the production of (*Z*)-but-2-enenitrile (**6**) greatly increases. However, by 10^{-1} bar, the principal product has become but-3-enenitrile (**13**). This is not surprising, because it would be one of the first-formed products from the radical-radical reaction, and the increased pressure provides a means of collisionally cooling it before it can react. Of some interest is the fact that cyanocyclopropane (**31**) becomes a detectable product at this pressure. Presumably, one is in a pressure regime whereby most of the initially formed but-3-enenitrile is collisionally quenched, but some fraction can still react. The reactions that do occur cannot progress much beyond one mechanistic step, though, because the products will also be collisionally cooled and if they are only barely above the threshold for reaction in their total energy, then collisional cooling will trap them in their local minima. Cyanocyclopropane is one of the intermediates that is a single mechanistic step away from but-3-enenitrile and so experiences this phenomenon. At the highest pressure, the first formed products from the radical-radical reaction are quenched almost immediately and so they form the only significant products.

Disappointingly, pyrrole is not a significant product at any of the pressures investigated. The largest amount formed was 0.75% at 0.025 bar. Had it not been for the fragmentation reactions at the lowest pressure, one might have expected the system eventually to make its way to pyrrole as the species with the lowest heat of formation. However, the fragmentations are effectively irreversible and so thwart that route to pyrrole. At higher pressure, when the fragmentations are suppressed, the system becomes trapped in local minima on the potential energy surface before reaching pyrrole. One must conclude, therefore, that the formation of pyrrole in ice grains [14] looks like the better route for extraterrestrial generation.

5 | Conclusions

The electronic-structure calculations in the present work have refined the results from previous investigations. In particular, two new intermediates in the mechanism for pyrrole pyrolysis have been identified. On the other hand, two previously proposed mechanistic steps have been argued not to be viable.

A master-equation kinetic analysis has shown that the principal products of pyrrole pyrolysis are not formed with first-order kinetics and so efforts to represent their appearance with first-order Arrhenius expressions are of limited value.

Using the same mechanistic scheme employed for pyrrole pyrolysis, the pressure-dependent kinetics of the allyl + •CN radical at low temperature have been simulated. The intent was to find out whether this reaction could provide an extraterrestrial route to pyrrole. Disappointingly, the conclusion is that it cannot. The one caveat to this conclusion is that at very low temperatures condensation or adsorption events may occur in the allyl + CN reaction, and these could not be included in the present simulation.

Author Contributions

Barry K. Carpenter: conceptualization, investigation, writing – original draft, methodology, validation, visualization, writing – review and editing, software, formal analysis, data curation.

Acknowledgments

The author would like to thank Dr. Robert Tranter of the Argonne National Laboratory for helpful discussion. Support of this work by Advanced Research Computing at Cardiff (ARCCA) is also gratefully acknowledged.

Data Availability Statement

All the data necessary to reproduce the calculations reported here are supplied in the Supporting Information for this paper.

References

1. J. M. Patterson, A. Tsamasfyros, and W. T. Smith, "Pyrolysis of Pyrrole," *Journal of Heterocyclic Chemistry* 5 (1968): 727–729.

2. A. Lifshitz, C. Tamburu, and A. Suslensky, "Isomerization and Decomposition of Pyrrole at Elevated Temperatures: Studies With a Single-Pulse Shock Tube," *Journal of Physical Chemistry* 93 (1989): 5802–5808.

3. J. C. Mackie, M. B. Colket, P. F. Nelson, and M. Esler, "Shock Tube Pyrolysis of Pyrrole and Kinetic Modeling," *International Journal of Chemical Kinetics* 23 (1991): 733–760.

4. M. Pelucchi, S. Arunthanayothin, Y. Song, et al., "Pyrolysis and Combustion Chemistry of Pyrrole, a Reference Component for Bio-Oil Surrogates: Jet-Stirred Reactor Experiments and Kinetic Modeling," *Energy & Fuels* 35 (2021): 7265–7284.

5. L. N. Wu, Z. Y. Tian, D. Wang, et al., "Dinitriles and Nitriles Are Common Intermediates of Pyrrole Pyrolysis," *Combustion and Flame* 245 (2022): 112358.

6. F. Dubnikova and A. Lifshitz, "Isomerization of Pyrrole. Quantum Chemical Calculations and Kinetic Modeling," *Journal of Physical Chemistry. A* 102 (1998): 10880–10888.

7. L. Zhai, H. F. Zhou, and R. F. Liu, "A Theoretical Study of Pyrolysis Mechanisms of Pyrrole," *Journal of Physical Chemistry. A* 103 (1999): 3917–3922.

8. M. Martoprawiro, G. B. Bacskay, and J. C. Mackie, "Ab Initio Quantum Chemical and Kinetic Modeling Study of the Pyrolysis Kinetics of Pyrrole," *Journal of Physical Chemistry. A* 103 (1999): 3923–3934.

9. G. B. Bacskay, M. Martoprawiro, and J. C. Mackie, "The Thermal Decomposition of Pyrrole: An Ab Initio Quantum Chemical Study of the Potential Energy Surface Associated With The Hydrogen Cyanide Plus Propyne Channel," *Chemical Physics Letters* 300 (1999): 321–330.

10. R. I. Kaiser, D. S. N. Parker, and A. M. Mebel, "Reaction Dynamics in Astrochemistry: Low-Temperature Pathways to Polycyclic Aromatic Hydrocarbons in the Interstellar Medium," *Annual Review of Physical Chemistry* 66 (2015): 43–67.

11. C. Eistrup, "A Chemical Modeling Roadmap Linking Protoplanetary Disks and Exoplanet Atmospheres," *ACS Earth and Space Chemistry* 7 (2023): 260–277.

12. E. V. F. de Aragao, P. X. Liang, L. Mancini, et al., "Dicyanoacetylene (NC_4N) Formation in the CN + Cyanoacetylene (HC_3N) Reaction: A Combined Crossed-Molecular Beams and Theoretical Study," *ACS Earth and Space Chemistry* 9 (2025): 2199–2214.

13. L. Mancini, G. Vanuzzo, P. Recio, et al., "Unveiling the Reaction Mechanism of the N((2)D) + Pyridine Reaction: Ring-Contraction Versus 7-Membered-Ring Formation Channels," *Journal of Physical Chemistry. A* 128 (2024): 7177–7194.

14. J. Wang, A. A. Nikolayev, J. H. Marks, et al., "Interstellar Formation of Nitrogen Heteroaromatics [Indole, C_8H_7N; Pyrrole, C_4H_5N; Aniline, $C_6H_5NH_2$]: Key Precursors to Amino Acids and Nucleobases," *Journal of the American Chemical Society* 146 (2024): 28437–28447.

15. I. A. Medvedkov, A. A. Nikolayev, S. J. Goettl, Z. H. Yang, A. M. Mebel, and R. I. Kaiser, "From the Laboratory to Space: Unveiling Isomeric Diversity of C5H2 in the Reaction of Tricarbon (C3, X1Σg+) With the Vinyl Radical (C2H3, X2A′)," *Chemical Science* 16 (2025): 17859–17866.

16. A. M. Thomas, M. Lucas, T. Yang, et al., "A Free-Radical Pathway to Hydrogenated Phenanthrene in Molecular Clouds-Low Temperature Growth of Polycyclic Aromatic Hydrocarbons," *ChemPhysChem* 18 (2017): 1971–1976.

17. B. Ruscic and D. H. Bross, "Active Thermochemical Tables v. 1.220," https://atct.anl.gov/Thermochemical%20Data/version%201.220/index.php. Accessed November 5, 2025.

18. L. Savi, M. T. Barreca, M. Bedogni, and F. Di Maiolo, *Journal of Chemical Theory and Computation* (2025, ASAP Article:), https://doi.org/10.1021/acs.jctc.5c01571.

19. N. J. DeYonker, T. Grimes, S. Yockel, et al., "The Correlation-Consistent Composite Approach: Application to the G3/99 Test Set," *Journal of Chemical Physics* 125 (2006): 104111.

20. T. V. Grimes, A. K. Wilson, N. J. DeYonker, and T. R. Cundari, "Performance of the Correlation Consistent Composite Approach for Transition States: A Comparison to G3B Theory," *Journal of Chemical Physics* 127 (2007): 154117.

21. X. F. Xu, I. M. Alecu, and D. G. Truhlar, "How Well Can Modern Density Functionals Predict Internuclear Distances at Transition States?" *Journal of Chemical Theory and Computation* 7 (2011): 1667–1676.

22. T. J. Lee and P. R. Taylor, "A Diagnostic for Determining the Quality of Single-Reference Electron Correlation Methods," *International Journal of Quantum Chemistry* 36 (1989): 199–207.

23. Y. Guo, K. Sivalingam, E. F. Valeev, and F. Neese, "Explicitly Correlated N-Electron Valence State Perturbation Theory (NEVPT2-F12)," *Journal of Chemical Physics* 147 (2017): 064110.

24. F. Neese, "Software Update: The ORCA Program System—Version 6.0," *Wiley Interdisciplinary Reviews: Computational Molecular Science* 15 (2025): e70019.

25. G. M. J. Barca, C. Bertoni, L. Carrington, et al., "Recent Developments in the General Atomic and Molecular Electronic Structure System," *Journal of Chemical Physics* 152 (2020): 154102.

26. M. W. Schmidt, K. K. Baldridge, J. A. Boatz, et al., "General Atomic and Molecular Electronic Structure System," *Journal of Computational Chemistry* 14 (1993): 1347–1363.

27. A. G. Dana, M. S. Johnson, J. W. Allen, et al., "Automated Reaction Kinetics and Network Exploration (Arkane): A Statistical Mechanics, Thermodynamics, Transition State Theory, and Master Equation Software," *International Journal of Chemical Kinetics* 55 (2023): 300–323.

Supporting Information

Additional supporting information can be found online in the Supporting Information section. **Data S1:** Supporting Information